

MambaTrack3D: A State Space Model Framework for LiDAR-Based Object Tracking under High Temporal Variation

Shengjing Tian, Yinan Han, Xiantong Zhao*, Xuehu Liu, and Qi Lang

Abstract—Dynamic outdoor environments with high temporal variation (HTV) pose significant challenges for 3D single object tracking in LiDAR point clouds. Existing memory-based trackers often suffer from quadratic computational complexity, temporal redundancy, and insufficient exploitation of geometric priors. To address these issues, we propose MambaTrack3D, a novel HTV-oriented tracking framework built upon the state space model Mamba. Specifically, we design a Mamba-based Inter-frame Propagation (MIP) module that replaces conventional single-frame feature extraction with efficient inter-frame propagation, achieving near-linear complexity while explicitly modeling spatial relations across historical frames. Furthermore, a Grouped Feature Enhancement Module (GFEM) is introduced to separate foreground and background semantics at the channel level, thereby mitigating temporal redundancy in the memory bank. Extensive experiments on KITTI-HTV and nuScenes-HTV benchmarks demonstrate that MambaTrack3D consistently outperforms both HTV-oriented and normal-scenario trackers, achieving improvements of up to +6.5 success / +9.5 precision over HVTrack under moderate temporal gaps. On the standard KITTI dataset, MambaTrack3D remains highly competitive with state-of-the-art normal-scenario trackers, confirming its strong generalization ability. Overall, MambaTrack3D achieves a superior accuracy–efficiency trade-off, delivering robust performance across both specialized HTV and conventional tracking scenarios.

Index Terms—Point Clouds, High Temporal Variation, Object Tracking, Deep Learning.

I. INTRODUCTION

The domain of visual information processing has been transitioning from two-dimensional (2D) camera pixels to three-dimensional (3D) geometric point clouds [1], [2], wherein Light Detection and Ranging (LiDAR) has been serving as a predominant sensor. Accordingly, visual object tracking (VOT) from the LiDAR point clouds also has been becoming indispensable to perceive the surrounding environments in the rapidly evolving fields of robotic vision [3], [4], autonomous driving [5], [6], and augmented reality [7]. The primary goal of the VOT is to employ a bounding box to estimate the pose and

Manuscript received –; revised –

Shengjing Tian is with the School of Economics and Management, China University of Mining and Technology, China. tye.dut@gmail.com

Yinan Han is with the DUT-BSU Joint Institute, Dalian University of Technology, China. Spolico_hyn@outlook.com

Xiantong Zhao are with the School of Mathematical Sciences, Dalian University of Technology, China. Corresponding author: xtongz.dut@gmail.com

Qi Lang are with the School of Information Science and Technology, Northeast Normal University, China. langqi@nenu.edu.cn

Xuehu Liu are with the School of Computer Science and Artificial Intelligence, Wuhan University of Technology, China. liuxuehu@whut.edu.cn

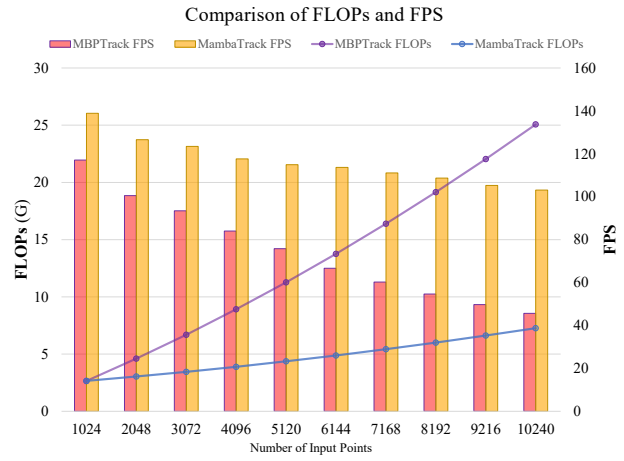


Fig. 1. Performance comparisons between transformer-based method and our method. The X-axis is the number of input points. The FLOPs on the left Y-axis reflects the computation complexity, while the FPS on the right Y-axis represents the running speed of different methods.

centroid of the object of interest within frame streams, facilitating systems in the real-time localization capacity within the 3D physical space. Recent research has increasingly focused on point clouds for 3D object detection and tracking [2], [8]. However, the majority of existing literature emphasizes accuracy in normative settings [9] [10] [11], often overlooking special scenarios where long intervals exist between two adjacent perceptions, called High Temporal Variation (HTV).

HTV tracking plays a pivotal role in real-world applications, as it can markedly decrease computational demands across a wide range of tasks, such as detection and segmentation, through the adoption of skipped-tracking strategies [12], [13]. Moreover, HTV tracking is essential for deployment on edge devices, such as Unmanned Aerial Vehicles, which are often constrained by limited point cloud resolution, computational capability, and power supply [13], [14]. To this end, the approaches for HTV tracking must be sufficiently efficient to tackle the following challenges: High Computational Efficiency (HCE), Large Appearance Variations (LAV), Distractions from Similar Objects (DSO), and Background Noise (BN). The HCE demands that the tracking algorithm operate at high frame rates to meet real-time requirements. The LAV affects the point density and spatial distribution of LiDAR data, typically arising from occlusions, rapid object motion, and environmental factors such as weather changes, which

may cause objects to be partially or fully obscured. The DSO is also inevitable because we necessitate an expansion of the 3D search area to accommodate substantial movements. This expansion increases the likelihood of interference from visually similar objects. Naturally, the enlargement of the search area inherently reduces the proportion of target-relevant information and amplifies the presence of background noise (BN) within the scene.

Current research in LiDAR VOT primarily leverages the Siamese paradigm [9], [15] to improve accuracy under normative settings. This framework takes a target template from the previous frame and a search area from the current frame as inputs, encoding them into a latent feature space to capture both global and local semantic information. It then renders the target surface points discriminative by integrating template information into the search area, ultimately followed by a localization network to estimate the target's state in the current frame. Although methods like P2B [9], STNet [10], and CX-Track [16] have made significant strides, they often struggle in high temporal variation scenarios. This limitation arises because these approaches only pass the target cue from the latest frame to the current one, without effectively leveraging historical frame information. To address this, several memory-based trackers [17] [18] [19] [11] have been proposed to perform tracking in point clouds. Among them, the most outstanding and representative tracker, MBPTrack [11], utilizes the Transformer [20] to process the rich temporal context across historical frames. However, under HTV conditions, these methods still face challenges in efficiently managing and utilizing sequential data. In light of this, HVTrack [21] specifically targets HTV scenarios by designing dedicated cross-attention and self-attention modules within a memory bank to deal with large appearance variations, similar object distractions, and background noise. Despite the advancements achieved by memory-based approaches, they exhibit limitations in terms of High Computational Efficiency (HCE) and temporal redundancy. Specifically, attention modules are detrimental to the HCE, as they incur quadratic computational complexity, thereby hampering runtime performance as the memory bank grows. Moreover, the aggregation of multiple historical frames tends to yield dense point clouds within the memory bank, introducing temporal redundancy and weakening the correlation between the template and the search region. Furthermore, transformer-based matching strategies in memory banks rely merely on the cosine similarity of point cloud features across various frames, frequently overlooking geometric priors of objects—such as spatial relationships among historical frames—that are crucial for precise tracking.

To address the aforementioned challenges, this paper proposes a point cloud tracking framework for high temporal variation (HTV) scenarios, built upon the state space model Mamba [22]. Specifically, to meet the demand for high computational efficiency in HTV tracking, we develop a novel spatiotemporal-aware inter-frame feature propagation module. This module offers two key advantages: 1) Unlike previous methods that rely on reference-free feature extraction(*e.g.*, directly applying PointNet++ or DGCNN), our module replaces feature extraction with inter-frame feature propagation, explic-

itly modeling the spatial relationships between the current and historical point clouds during the propagation process. 2) In contrast to the quadratic computational complexity of Transformer-based architectures, our module is based on a linear-time sequence model, which can achieve over 110 FPS and is four times faster than existing HTV tracking methods. To further mitigate the temporal redundancy in the memory bank, we propose a grouped feature enhancement module that exploits foreground–background collaboration. The resulting features can facilitate distinguishing the correlated points between the current frame and the memory bank, further alleviating temporal redundancy caused by aggregating historical frames. We evaluate the proposed method on the KITTI dataset under high temporal variation settings, and the tracking results demonstrate significant performance improvements.

To sum up, the contributions of this study are threefold:

- A more efficient tracking framework is proposed for 3D HTV tracking, which utilizes the state space model to revolute the conventional single-frame feature extraction into multiple-frame feature propagation.
- A grouped feature enhancement module is proposed to capture foreground and background semantics, which leverages two grouped channel experts to learn discriminative features and degrade temporal redundancy.
- A superior accuracy–speed trade-off is achieved, with the proposed method delivering considerable accuracy gains and a 2× runtime improvement in HTV scenarios over the current state-of-the-art, while maintaining competitive performance under normal settings.

II. RELATED WORK

Visual object tracking from the LiDAR point clouds has attracted much attention from researchers, attributed to its wide range of applicable scenarios. In this section, we systematically examine 3D tracking in a normal setting, followed by a discussion of 3D tracking in a specific setting. Lastly, we review the application of optimal transport theory within the domain of vision.

A. 3D Tracking in Normal Settings

For the understanding of LiDAR data in outdoor environments, Giancola *et al.* [15] pioneered the use of pointnet [23] to compute the appearance features of candidate point cloud segments and track the target based on the Siamese framework. Subsequent advancements in this field have incorporated sophisticated methodologies aimed at enhancing tracking accuracy. Within this conceptual paradigm, P2B [9] accomplishes an end-to-end architecture design, utilizing a deep Hough vote-based localization [24] and feature fusion between the target and the search area. BAT [25] augments the fusion by employing box clouds to derive a nine-dimensional representation for each raw point to the vertex of the bounding box. Researchers have subsequently focused on three key aspects: feature extraction, feature fusion, and localization mechanisms. Hui *et al.* [10] introduced a Siamese Transformer network which improves the local feature extraction method. Conversely, Shan *et al.* [26] employed Transformer networks

to integrate target information in feature fusion through cross-attention mechanisms. Park *et al.* [27] utilized the graph neural network to propagate information between template and search area features. Considering the bird’s-eye view’s (BEV) capability in capturing motion, Luo *et al.* [28] utilized the BEV as an ancillary branch for feature representation to enhance the tracking process. Hui *et al.* [29] focused on the localization module and replaced the traditional vote-based method with a BEV-based response map, where each “pixel” acts as an anchor point to facilitate the generation of candidate enclosing boxes. Xu *et al.* [16] and Guo *et al.* [30] posited that the spatial relationship of the target with respect to other objects within the background can serve as referential clues to mitigate the influence of interfering objects.

In addition to the above appearance-based methods, motion-based approaches predict the approximate center of the target in the current frame utilizing historical frame data, which can serve as prior knowledge to enhance the precision of final bounding-box predictions. M2Tracker [31] and P2P [32] utilizes single-frame historical data in conjunction with a template to estimate the motion offset between frames. In contrast, DMT [33] utilizes multi-frame historical data and integrates it with the target template, generating the target’s bounding box by deep Hough voting [24].

While recent breakthroughs have made notable progress in the LiDAR VOT, existing methods often struggle in scenarios characterized by large appearance changes. This limitation stems from the propensity of these methods to solely transfer the target cue from the previous frame to the current frame, neglecting to harness the rich contextual information available in historical frames. To overcome this shortcoming, a new class of memory-based trackers has emerged [17] [18] [19] [11], specifically designed to leverage temporal context to enhance tracking performance in point cloud. TAT [17] employs historical templates to develop target-specific features through processes of sampling, enhancement, and aggregation operations. MBPTrack [11] introduces a memory bank module that disseminates target information across multiple historical frames into the search area. SeqTrack3D [19] and StreamTrack [34] sequentially integrate information from multiple point cloud frames, thereby reformulating the tracking task as a sequence processing problem. In particular, SeqTrack3D [19] employs bounding box sequences predicted from the preliminary stage to guide the learning of point cloud sequence features, utilizing historical bounding boxes as constraints to regulate the network’s modeling of target motion patterns. StreamTrack [34] adopts a hybrid attention mechanism to carefully extract the spatial and temporal information from point cloud sequences. The aforementioned methods primarily address tracking in normal settings.

B. 3D Tracking in Specialized Settings

In fact, tracking in specialized scenarios, such as distant and small objects, adverse weather conditions, high temporal variations, and adversarial attacks, is also highly prevalent. In such settings, the performance of the aforementioned methods often degrades markedly. Tian *et al.* [35] observed that

the current trackers suffer from significant degradation when conducting class-agnostic tracking, and thus proposed the generation of a common pattern throughout the feature fusion process. Similarly, the challenges posed by distant and small objects were tackled in [36] through the design of a prototype feature and subdivision modules to emphasize foreground targets. Dreissig *et al.* [37] investigated the vulnerability of the LiDAR perception algorithms in conditions of rain, snow, and fog. Tian *et al.* [38] evaluated the robustness of three main tracking frameworks, specifically in the presence of white-box and black-box attacks. For high temporal variations, Wu *et al.* [21] introduced a pose-aware memory bank to handle large shape changes, similar object distractions, and background noise. In this work, we also concentrate on high temporal variation tracking task, and aim to mitigate the following limitations of previous studies: insufficient computational efficiency, temporal redundancy in the memory bank, and the lack of historical geometric prior in feature extraction.

C. State Space Models for Information Processing

Mamba model [22], [39], introduced by Gu and Dao, is a state space model designed for efficient long-sequence modeling derived from the continuous system. Building on the S4 framework [40], it introduces an input-dependent selection mechanism and a hardware-friendly selective scan, enabling efficient long-range dependency modeling with near-linear complexity. Initially applied to 1D sequences, Mamba has been adapting to 2D vision tasks [41], [42]. MambaVision [41] introduces a vision-friendly Mamba block within a hybrid Mamba–Transformer backbone that combines CNN-based early stages with self-attention in later layers, achieving advanced accuracy–throughput trade-offs and superior performance across classification, detection, and segmentation benchmarks. However, applying Mamba to 3D point clouds poses challenges: (1) unordered point sets can cause pseudo-order dependence; (2) point cloud understanding relies on fine-grained local geometric structures, which are not explicitly captured by the original Mamba design; and (3) global–local feature integration is non-trivial. Several works have explored Mamba for 3D point cloud classification and detection [43]–[46]. Specifically, PointMamba [43] directly models point patch sequences but lacks explicit local geometry; PCM [45] integrates Mamba into PointMLP but with high computational cost; Mamba3D [46] introduces Local Norm Pooling for local geometry and a bidirectional SSM to mitigate pseudo-order effects, achieving state-of-the-art results with linear complexity. Although these Mamba-based point cloud classification methods hold promise as backbones for 3D HTV tracking, they still face challenges in streaming point cloud video scenarios and lack dedicated tracking-oriented designs to address temporal redundancy in the memory bank and the incorporation of historical geometric priors.

III. METHOD

Our method aims to deal with the three challenges that are suffered in HTV scenarios:

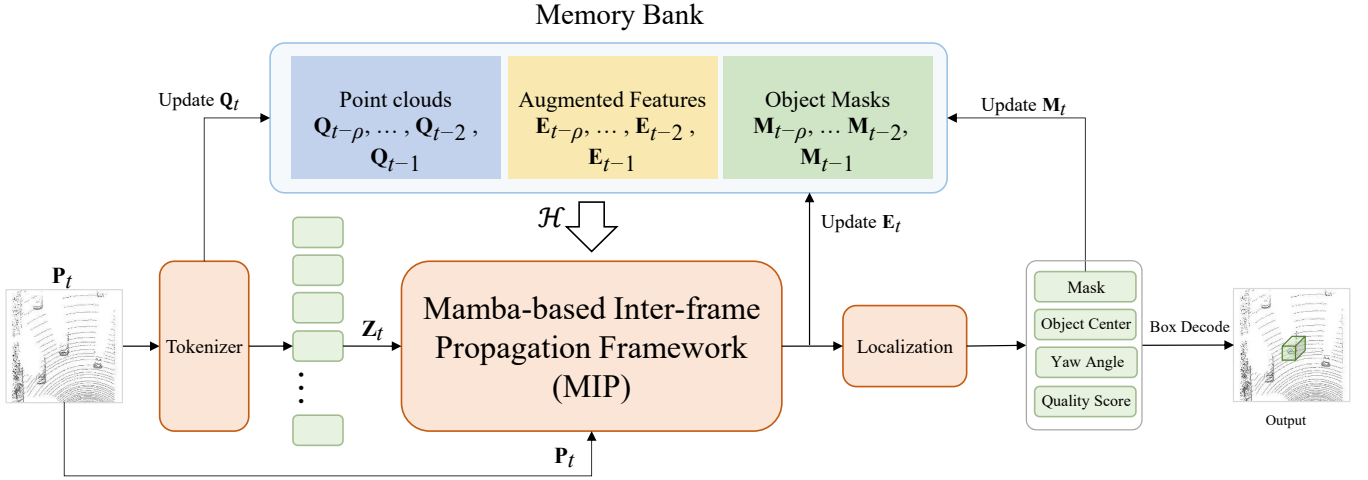


Fig. 2. The overall pipeline of the proposed method.

- Q1: How to improve the computational efficiency from the existing quadratic complexity;
- Q2: How to improve the tracking accuracy with consideration of spatial relationships among historical frames;
- Q3: How to mitigate temporal redundancy.

In the following subsections, we will first formulate the LiDAR VOT into a mathematical problem. Then, we will present a Mamba-based inter-frame propagation framework, which is capable of improving run speed without sacrificing tracking accuracy. Finally, we will introduce a grouped feature enhancement module to alleviate temporal redundancy.

A. Problem Definition

To conduct visual object tracking from the LiDAR data, the task begins by identifying a specific target within a 3D bounding box in the first frame of a point cloud sequence. Each frame is represented as a point cloud $P_t \in \mathbb{R}^{N_t \times 3}$, where N_t denotes the number of points at time t . The target bounding box is parameterized by its center coordinates (x, y, z) , size (w, l, h) , and heading angle θ around the up-axis.

Formally, given an initial point cloud P_1 and the object of interest covered by the 3D bounding box B_1 , the goal is to recursively estimate the 7-degree-of-freedom state $\mathbf{B}_t = (x_t, y_t, z_t, w_t, l_t, h_t, \theta_t)$ in each subsequent frame P_t for $t = 2, \dots, T$. In transportation scenarios, most elements on the road are usually rigid, thus their physical sizes (w, l, h) remain unchanged in 3D space. Taking the point cloud sequences as input, the LiDAR VOT simplifies to estimating the translational offsets $(\delta_t^x, \delta_t^y, \delta_t^z)$ and the angular offset δ_t^θ online. In this study, the proposed approach leverages sequential modeling through a deep learning-based state estimator that incorporates historical context into the current search region. The process can be formulated as:

$$\Phi(P_t; \mathcal{H}) \mapsto (\delta_t^x, \delta_t^y, \delta_t^z, \delta_t^\theta), \quad (1)$$

where \mathcal{H} encodes historical target states and environments, enabling robust and accurate tracking through temporal reasoning.

B. Mamba-based Inter-frame Propagation Framework

In this subsection, we first provide a brief overview of Mamba, and then present the detailed design of the Mamba-based Inter-frame Propagation (MIP) framework.

Mamba Review. State space model is used to represent the dynamic behavior of a system over time. Its state equation can be written as $h'(t) = Ah(t) + Bx(t)$. For implementation in computer programming, it is discretized using the Zero-Order Hold method into an iterative form: $h_{k+1} = \bar{A}h_k + \bar{B}x_k$, where $\bar{A} = \exp(A\Delta)$ and $\bar{B} = A^{-1}(\exp(A\Delta) - I)B$, and $\Delta = t_{k+1} - t_k$. Considering the output projection matrix \bar{C} , the final output y can be achieved in a parallel computation manner using a convolution operation: $y = \mathbf{x} * K$, where $K = (\bar{C}\bar{A}^0\bar{B}, \bar{C}\bar{A}^1\bar{B}, \dots, \bar{C}\bar{A}^k\bar{B})$ and $\mathbf{x} = (x_0, x_1, \dots, x_k)$.

After training, however, the parameters \bar{A} , \bar{B} , and \bar{C} are fixed, which prevents the model from being input-aware and limits its ability to selectively retain attention. Therefore, Mamba introduces an input-dependent dynamic weight learning mechanism and incorporates a hardware-aware selective scanning algorithm [22] to enable parallel computation: $h_{k+1} = \hat{A}(x_k)h_k + \hat{B}(x_k)x_k$. Please refer to [22] for more details.

The MIP. Although Transformer-based architectures have achieved impressive results on the LiDAR VOT, their quadratic complexity poses a significant limitation for real-time applications. As illustrated in Fig. 1, when the input quantity of point clouds increases, the Transformer-based methods (e.g., MBPTrack [11]) suffer from a sharp rise in both computational cost and runtime latency. To enable efficient computation listed in the Q1, we deal with the LiDAR VOT based on the state space model, Mamba, which excels at near-linear complexity. Furthermore, to enhance tracking accuracy stated in the Q2, we design a feature propagation mechanism that exploits both spatial relationships and temporal historical information, in contrast to conventional single-frame feature extraction. The integration of these two ideas constitutes the core motivation behind our MIP.

The figure 3 illustrates the MIP framework. The input

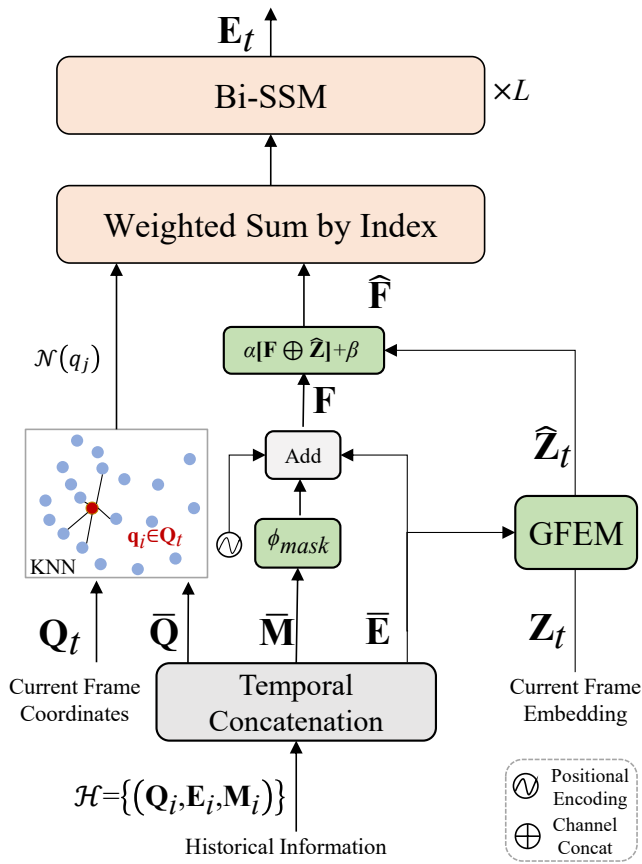


Fig. 3. The pipeline of the proposed MIP module.

consists of two components: the current frame \mathbf{P}_t and the memory bank \mathcal{H} . On one hand, as the input of the state space model, “tokens” are first obtained from the point cloud:

$$\mathbf{Z}_t = \mathcal{K}(\mathcal{S}(\mathbf{P}_t)), \quad (2)$$

where \mathcal{S} means farthest point sampling and \mathcal{K} utilizes mini-PointNet [23] to learn the local feature of each sampled point within its K-Nearest Neighborhood (KNN). On the other hand, to fully leverage temporal historical cues, the memory bank \mathcal{H} is spanned by three basic elements: point cloud coordinates $\mathbf{Q}_i = \mathcal{S}(\mathbf{P}_i)$, features \mathbf{E}_i , and target masks \mathbf{M}_i . It can be written as $\mathcal{H} = \{(\mathbf{Q}_i, \mathbf{E}_i, \mathbf{M}_i) \mid \mathbf{Q}_i \in \mathbb{R}^{\hat{N} \times 3}, \mathbf{E}_i \in \mathbb{R}^{\hat{N} \times C}, \mathbf{M}_i \in \mathbb{R}^{\hat{N} \times 1}, i = t - \rho, t - \rho + 1, \dots, t - 1\}$. Herein, ρ represents the number of past frames stored in the memory bank.

Based on the above inputs, we first concatenate the historical frames in temporal order:

$$\bar{\mathbf{Q}} = [\mathbf{Q}_{t-\sigma}; \dots; \mathbf{Q}_{t-2}; \mathbf{Q}_{t-1}], \quad (3)$$

$$\bar{\mathbf{E}} = [\mathbf{E}_{t-\sigma}; \dots; \mathbf{E}_{t-2}; \mathbf{E}_{t-1}], \quad (4)$$

$$\bar{\mathbf{M}} = [\mathbf{M}_{t-\sigma}; \dots; \mathbf{M}_{t-2}; \mathbf{M}_{t-1}]. \quad (5)$$

The goal is to exploit historical cues to obtain more discriminative target features for the current frame \mathbf{Q}_t . Prior to feature propagation, the mask features $\bar{\mathbf{M}}$ are integrated into the appearance features $\bar{\mathbf{E}}$:

$$\mathbf{F} = \bar{\mathbf{E}} + \phi_{mask}(\bar{\mathbf{M}}), \quad (6)$$

where $\phi_{mask} : \mathbb{R}^{\rho\hat{N} \times 1} \mapsto \mathbb{R}^{\rho\hat{N} \times C}$ is a 1D convolution that learns mask-aware representations.

For each point $q_j \in \mathbf{Q}_t$, we construct its local neighborhood $\mathcal{N}(q_j)$ in the aggregated historical point cloud $\bar{\mathbf{Q}}$ using KNN. The corresponding historical features $\{\mathbf{F}_k \mid k \in \mathcal{N}(q_j)\}$ are then retrieved from \mathbf{F} . The propagated feature of q_j is computed as:

$$\mathbf{e}_{t,j} = \sum_{k \in \mathcal{N}(q_j)} \omega_k \odot \hat{\mathbf{F}}_k, \quad (7)$$

$$\hat{\mathbf{F}}_k = \alpha[\mathbf{F}_k \oplus \mathbf{Z}_t(q_j)] + \beta, \quad (8)$$

$$\omega_k = \frac{\exp(\hat{\mathbf{F}}_k)}{\sum_{l \in \mathcal{N}(q_j)} \exp(\hat{\mathbf{F}}_l)}, \quad (9)$$

$$\mathbf{E}_t = [\mathbf{e}_{t,1}, \mathbf{e}_{t,2}, \dots, \mathbf{e}_{t,\hat{N}}], \quad (10)$$

where \odot denotes element-wise multiplication, \oplus denotes channel concatenation, $\mathbf{z}_t(q_j) \in \mathbb{R}^C$ is the initial token embedding of the current point, and α, β are learnable parameters.

Finally, the propagated features are fed into Bi-SSM [46], which effectively handles unordered and irregular point sets:

$$h_{k+1} = \hat{A}(\mathbf{e}_{t,j})h_k + \hat{B}(\mathbf{e}_{t,j})\mathbf{e}_{t,j}. \quad (11)$$

C. Grouped Feature Enhancement Module

In fact, the redundancy stated in the Q3 can be alleviated by constructing such local neighborhoods in historical frames and selecting top-K keypoints. However, redundant information stored in the memory bank may reduce the discriminative power of the features computed within local neighborhoods. To further address the Q3, we enhance the representation of foreground and background points from the perspective of feature channels. Our underlying motivation is that each feature channel should be dedicated to a single category of points (either foreground or background) [35]. Specifically, based on Eq. (8), it can be observed that point cloud features of the current frame are primarily generated through propagation from historical frame features. We divide the features into two groups and apply distinct linear transformations to process foreground and background points separately.

Specifically, given $\mathbf{E}_t \in \mathbb{R}^{\hat{N} \times C}$ and $\bar{\mathbf{E}} \in \mathbb{R}^{\rho\hat{N} \times C}$, we split them into two channel groups: $\mathbf{Z}_t^1, \mathbf{Z}_t^2 \in \mathbb{R}^{\hat{N} \times \frac{C}{2}}$ and $\bar{\mathbf{E}}^1, \bar{\mathbf{E}}^2 \in \mathbb{R}^{\rho\hat{N} \times \frac{C}{2}}$. For each group, cross-attention is performed as follows:

$$\hat{\mathbf{Z}}_t^1 = \text{softmax}[(\mathbf{Z}_t^1 \mathbf{W}_Q^1)(\bar{\mathbf{E}}^1 \mathbf{W}_K^1)^\top](\bar{\mathbf{E}}^1 \mathbf{W}_V^1), \quad (12)$$

where $\mathbf{W}_Q^1, \mathbf{W}_K^1, \mathbf{W}_V^1$ are learnable parameter matrices. Similarly, $\hat{\mathbf{E}}_t^2$ can be computed in the same manner. Concatenating the two groups along the channel dimension yields $\mathbf{E}_t = \hat{\mathbf{Z}}_t^1 \oplus \hat{\mathbf{Z}}_t^2$. Consequently, Eq. (8) is reformulated as:

$$\hat{\mathbf{F}}_k = \alpha[\mathbf{F}_k \oplus \hat{\mathbf{Z}}_t(q_j)] + \beta. \quad (13)$$

These enhanced representations improve the discrimination of correlated points across the current frame and the memory bank, effectively reducing the temporal redundancy accumulated from historical frame aggregation.

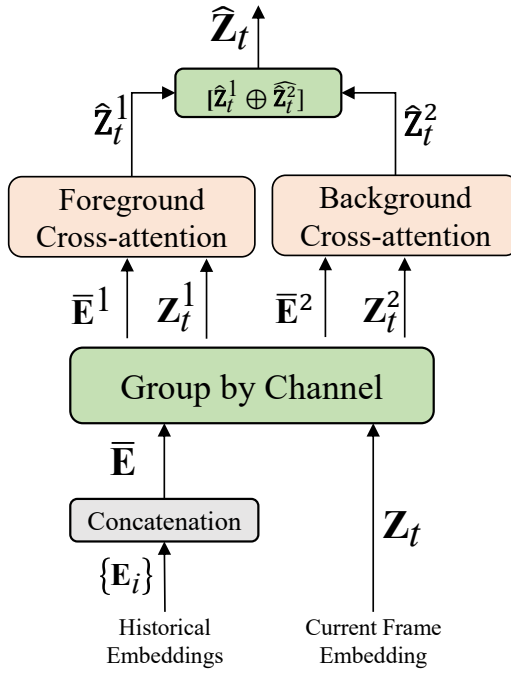


Fig. 4. The pipeline of the proposed GFEM module.

D. Implementation Details

The features processed by the MIP and GFEM modules are finally fed into a box-Prior localization network [11]. The outputs of this network include: foreground–background classification results for the current frame, Hough voting–based center predictions and their quality scores, and the parameters of the 3D bounding box along with their quality scores. The loss function follows the same formulation as in MBPTrack:

$$\mathcal{L} = \mathcal{L}_m + \mathcal{L}_c + \mathcal{L}_q + \mathcal{L}_s + \mathcal{L}_b, \quad (14)$$

where \mathcal{L}_m is a cross-entropy loss constraining the generation of the foreground–background mask, \mathcal{L}_c is a mean squared error loss supervising the Hough voting center prediction, \mathcal{L}_q and \mathcal{L}_s are cross-entropy losses supervising the quality scores of the Hough voting and bounding box respectively, and \mathcal{L}_b is a smooth-L1 loss constraining the bounding box parameters.

For inter-frame propagation training, we sample target segments of 8 consecutive frames from LiDAR point cloud sequences, with each segment serving as a training instance. During token generation, the number of tokens per frame is set to $\hat{N} = 128$, and the feature dimension is set to $C = 128$. The memory bank size is fixed at $\rho = 3$. For each point q_j , the neighborhood set $\mathcal{N}(q_j)$ is constructed with 4 nearest neighbors.

IV. EXPERIMENTS

A. Datasets and Metrics

Datasets. In this study, we conduct experiments on outdoor point cloud data collected by LiDAR sensors. KITTI [6] and nuScenes [8] are two representative large-scale outdoor datasets that provide 3D bounding box annotations of object

instances over time, making them widely used benchmarks for training and evaluating tracking algorithms.

The KITTI dataset was collected using a 64-beam LiDAR sensor, capable of capturing more than 1.3 million points per second at a frequency of 10 Hz. We adopt the KITTI Tracking benchmark, which consists of 21 scenes covering diverse environments such as roadways, residential areas, and campuses. This dataset provides frame-by-frame annotations. To evaluate the robustness of our method under high temporal variation, we follow the sampling strategy in [21], where each tracking sequence is subsampled at different frame intervals. Specifically, we set the sampling intervals to 2, 3, 5, and 10 frames to comprehensively assess performance under varying temporal gaps.

The nuScenes dataset was collected using a 32-beam LiDAR operating at 20 Hz, capturing up to 1.4 million points per second. It contains 1000 driving scenes, each lasting approximately 20 seconds. Due to the high cost of annotation, only key frames are labeled, with one frame annotated every 0.5 seconds. The differences between these two LiDAR sensors (64-beam vs. 32-beam, dense vs. sparse sampling) provide a more comprehensive evaluation of the adaptability and robustness of the proposed tracking algorithm.

Evaluation metrics. For the evaluation metrics, the success and precision rates were used, following the framework of a one-pass evaluation [47]. The success rate is represented in the area under the curve (AUC) plot, where the X-axis denotes the intersection over union (IOU) between the predicted and ground-truth bounding boxes, and the Y-axis indicates the proportion of frames exceeding the specified threshold. The IOU value is measured on a continuous scale from 0 to 1. Conversely, the precision is also calculated through an AUC plot; in this case, the X-axis measures the center errors between the predictions and ground-truth, while the Y-axis quantifies those frames where the center error falls below a certain threshold.

B. Main Results on High Temporal Variation

Current LiDAR-based tracking methods can be divided into two categories: those designed for normal scenarios and those tailored for specialized scenarios. This work focuses on the latter, specifically high temporal variation (HTV) tracking. HVTrack is the pioneering baseline for this task, and we adopt it as our reference model, aiming to improve accuracy through efficient utilization of temporal and geometric information. To comprehensively validate our approach, denoted as MambaTrack, we also evaluate it under HTV settings against state-of-the-art trackers originally developed for normal scenarios, including P2B [9], BAT [25], M2Track [31], CXTrack [16], M3SOT [48], and MBPTrack [11]. Detailed results on the KITTI and nuScenes datasets are analyzed in the following subsections.

Results on KITTI-HTV. At 2-frame intervals, MambaTrack3D achieves the best mean performance of 67.2/85.0, improving over HVTrack by +4.5/+5.7. This indicates that our framework effectively leverages temporal and geometric cues to enhance discriminability when temporal gaps are

TABLE I

COMPARISON OF MAMBATRACK3D WITH THE STATE-OF-THE-ART METHODS ON EACH CATEGORY OF THE KITTI-HTV DATASET. THE KITTI-HTV DATASET IS CONSTRUCTED FOR TRAINING AND TESTING BY SAMPLING DIFFERENT FRAME INTERVALS IN THE KITTI DATASET. **BOLD** DENOTES THE BEST RESULTS. “SUCCESS/PRECISION” ARE USED FOR EVALUATION. IMPROVEMENT AND DETERIORATION ARE SHOWN IN **GREEN** AND **RED**, RESPECTIVELY.

Methods (Frame Number)	2 Intervals					3 Intervals				
	Car (6424)	Pedestrian (6088)	Van (1248)	Cyclist (308)	Mean (14068)	Car (6424)	Pedestrian (6088)	Van (1248)	Cyclist (308)	Mean (14068)
P2B [9]	56.3/71.0	30.8/53.0	33.4/38.4	41.8/61.4	42.9/60.1	43.4/51.8	27.9/46.8	27.9/31.8	44.8/64.4	35.4/48.1
BAT [25]	61.8/74.2	36.5/61.1	26.8/30.4	54.1/78.7	47.6/64.7	51.7/61.9	31.8/53.5	24.0/28.2	50.5/72.6	40.6/55.5
M2Track [31]	63.0/76.6	54.6/81.7	52.8/66.5	68.3/89.3	58.6/78.2	62.1/72.7	51.8/74.3	33.6/41.6	64.7/82.0	55.1/70.8
CXTrack [16]	61.4/70.9	62.6/86.3	56.0/69.1	59.2/76.9	61.4/77.5	47.4/53.1	57.9/79.3	48.5/58.8	40.7/58.4	51.9/65.1
M3SOT [48]	59.0/67.9	61.7/86.3	55.2/68.7	55.1/86.3	59.8/76.3	46.9/52.6	50.1/74.0	43.3/53.7	32.4/48.1	47.7/61.9
MBPTrack [11]	70.3/80.2	58.6/81.5	50.7/59.7	65.5/82.0	63.4/79.0	64.3/73.3	48.2/69.7	43.6/50.0	68.6/86.6	55.6/70.0
HVTrack [21]	67.1/77.5	60.0/84.0	50.6/61.7	73.9/93.6	62.7/79.3	66.8/76.5	51.1/71.9	38.7/46.9	66.5/89.7	57.5/72.2
Ours	70.0/81.9	64.3/89.5	64.2/76.2	77.3/94.8	67.2/85.0	69.5/80.9	59.5/85.6	56.8/65.7	69.6/88.1	64.0/81.7
					$\uparrow 4.5 / \uparrow 5.7$					$\uparrow 6.5 / \uparrow 9.5$
Methods (Frame Number)	5 Intervals					10 Intervals				
	Car (6424)	Pedestrian (6088)	Van (1248)	Cyclist (308)	Mean (14068)	Car (6424)	Pedestrian (6088)	Van (1248)	Cyclist (308)	Mean (14068)
P2B [9]	39.3/46.1	27.4/43.5	27.2/30.4	35.0/44.4	33.0/43.5	28.6/29.2	23.1/31.1	25.9/27.3	29.1/28.3	26.0/29.8
BAT [25]	44.1/51.1	21.1/32.8	26.1/29.5	35.7/46.3	32.4/41.1	30.6/33.1	21.7/29.2	20.8/20.7	29.3/29.1	25.9/30.2
M2Track [31]	50.9/58.6	31.6/45.4	30.0/36.5	47.4/61.0	40.6/51.0	33.0/35.1	17.5/24.1	20.7/20.8	27.7/26.6	25.0/28.9
CXTrack [16]	38.6/42.2	35.0/47.8	21.6/24.3	25.7/33.3	35.3/42.8	30.2/32.4	18.2/21.4	17.5/17.9	27.7/26.5	23.8/26.2
M3SOT [48]	30.5/34.5	31.0/44.0	18.3/21.0	21.6/25.9	29.4/37.2	26.1/26.6	16.2/18.8	17.6/17.1	27.5/26.2	21.1/22.4
MBPTrack [11]	54.9/61.7	37.6/56.3	23.7/25.3	36.9/43.8	44.3/55.7	32.1/33.3	22.3/28.5	18.5/17.3	27.5/26.2	26.6/29.6
HVTrack [21]	60.3/68.9	35.1/52.1	28.7/32.4	58.2/71.7	46.6/58.5	49.4/54.7	22.5/29.1	22.2/23.4	39.5/45.4	35.1/ 40.6
Ours	62.7/72.7	39.5/60.1	49.6/55.5	47.4/59.6	51.2/65.4	49.1/54.3	22.1/28.1	28.8/29.6	34.7/38.7	35.3/40.4
					$\uparrow 4.6 / \uparrow 6.9$					$\uparrow 0.2 / \downarrow 0.2$

small. At 3-frame intervals, the advantage becomes even more pronounced: MambaTrack3D reaches 64.0/81.7, outperforming HVTrack by +6.5/+9.5. This demonstrates strong robustness to moderate temporal variation, where conventional trackers degrade more sharply. As the temporal gap widens, performance drops for all methods at 5-frame intervals. However, MambaTrack3D still achieves the best mean score of 51.2/65.4, surpassing HVTrack by +4.6/+6.9. At the most challenging 10-frame interval, both methods experience significant degradation. The improvement is subtle, demonstrating that both trackers struggle under extreme temporal gaps, but MambaTrack3D maintains competitive stability. We observe that a similar distribution of training samples can facilitate tracking performance. For example, when using the model trained on cars to track vans, the improvement is particularly significant, with MambaTrack3D achieving 49.6/55.5 compared to 28.7/32.4 for HVTrack. These results highlight the advantages of HTV-oriented designs in maintaining robustness under large temporal gaps and demonstrate the cross-category adaptability of MambaTrack3D.

In addition, from the perspective of tracker categories, we further summarize the following findings:

- Both normal-scenario trackers and high temporal variation (HTV) trackers exhibit performance degradation as the frame interval increases. However, the degradation is more severe for normal-scenario trackers due to the lack of dedicated designs for temporal variation.
- HTV-oriented trackers (e.g., MambaTrack3D and HVTrack) consistently outperform normal-scenario trackers (e.g., BAT and M2Track) across all intervals. For instance, MambaTrack3D achieves 62.7/72.7 at a 5-frame interval, which is comparable to the performance of the normal-scenario tracker M3SOT at only a 2-frame interval (59.0/67.9).

Results on nuScene-HTV. The nuScenes dataset contains the tracklets where objects are annotated with bounding boxes per 10 frame intervals. Notably, its inherent sparsity (32-beam vs 64-beam) amplifies tracking challenges, particularly for small objects like pedestrians. MambaTrack3D achieves the best mean success/precision of 59.6/72.8, outperforming

TABLE II

COMPARISON OF MAMBATRACK3D WITH THE STATE-OF-THE-ART METHODS ON EACH CATEGORY OF THE NUSCENES DATASET. IMPROVEMENT AND DETERIORATION ARE SHOWN IN GREEN AND RED, RESPECTIVELY.

Type of Trackers	Methods (Frame Number)	Car (64159)	Pedestrian (33227)	Truck (13587)	Trailer (3352)	Bus (2953)	Mean (117278)
Normal Tracking	SC3D [15]	22.3/21.9	11.3/12.7	30.7/27.7	35.3/28.1	29.4/24.1	20.7/20.2
	P2B [9]	38.8/43.2	28.4/52.2	43.0/41.6	49.0/40.1	33.0/27.4	36.5/45.1
	BAT [25]	40.7/44.3	28.8/53.3	45.3/42.6	52.6/44.9	35.4/28.0	38.1/45.7
	M2Track [31]	55.9/65.1	32.1/60.9	57.4/59.5	57.6/58.3	51.4/51.4	49.2/62.7
	CXTrack [16]	44.6/50.5	31.5/55.8	51.3/50.7	59.7/53.6	42.6/37.3	42.0/51.8
	MBPTrack [11]	62.4/70.4	45.3/74.0	62.2/63.3	65.1/61.3	55.4/51.8	57.4/69.8
Temporal variation Tracking	HVTrack [21]	55.9/62.9	41.3/67.6	55.6/55.2	52.0/40.2	36.3/41.6	51.1/62.2
	Ours	64.9/73.8	47.1/76.2	64.2/66.6	65.7/60.4	59.8/56.5	59.6/72.8
↑ 8.5 / ↑ 10.6							

HVTrack by +8.5/+10.6. This substantial margin demonstrates our propagation and grouped feature enhancement modules effectively capture large-scale structural cues. Despite being small and sparse, MambaTrack3D achieves 47.1/76.2 in pedestrians, improving over HVTrack (41.3/67.6). This indicates stronger adaptability to deformable and low-density targets. The largest improvement is observed in the bus category, with MambaTrack3D reaching 59.8/56.5 compared to HVTrack's 36.3/41.6. This demonstrates the advantage of incorporating geometric priors for objects with large intra-class variations. In addition, MambaTrack3D consistently surpasses all normal-scenario trackers (e.g., MBPTrack, M2Track, CXTrack) across every category. For example, compared to MBPTrack, which is the strongest among normal trackers (57.4/69.8), MambaTrack3D still improves by +2.2/+3.0 in mean performance. This highlights that designs tailored for high temporal variation are crucial for robust tracking in sparse LiDAR settings.

C. Efficiency Comparison

To further evaluate the computational efficiency of the proposed MambaTrack3D, we compare its FLOPs and FPS with the representative Transformer-based tracker MBPTrack under different numbers of input points, as shown in Fig. 1.

Runtime speed (FPS). Across all input sizes, MambaTrack3D consistently achieves higher FPS than MBPTrack. For example, when the number of input points reaches 8192, MambaTrack3D still maintains real-time performance at 100 FPS, whereas MBPTrack drops significantly below this threshold. This demonstrates the advantage of the linear-time state space model over the quadratic complexity of Transformer-based architectures.

Computational complexity (FLOPs). The FLOPs of MambaTrack3D grow much more slowly with increasing input points compared to MBPTrack. While MBPTrack exhibits a sharp quadratic rise in FLOPs, MambaTrack3D maintains near-linear growth, confirming the theoretical efficiency of the proposed inter-frame propagation design.

Importantly, the superior runtime efficiency of MambaTrack3D does not come at the cost of accuracy. As shown

in the previous sections, MambaTrack3D achieves consistent improvements in success and precision across KITTI-HV and nuScenes-HV benchmarks, while simultaneously reducing computational overhead. These results highlight that MambaTrack3D achieves a favorable accuracy–efficiency trade-off, making it more suitable for real-time deployment in resource-constrained platforms.

D. Result Visualization

Fig.5 presents a progressive comparison between MambaTrack3D and MBPTrack across increasing temporal intervals (1, 2, 3, 5, and 10 frames). The visualization highlights how each tracker responds to growing temporal gaps and appearance variations in dynamic 3D point cloud environments.

At short intervals (1 frame), both methods closely follow the ground-truth bounding boxes, indicating reliable performance under minimal appearance change. However, as the interval increases to 2-3 frames, MBPTrack begins to accumulate positional drift, with bounding boxes gradually deviating from the true object location. In contrast, MambaTrack3D maintains accurate alignment by leveraging dynamic keypoint selection and optimal transport matching. At 5-frame intervals, MBPTrack fails to recover from abrupt object motion (e.g., lane changes), resulting in complete tracking loss. MambaTrack3D, however, continues to track successfully by exploiting spatial distribution priors and selective historical points based on the MIP module. Under the most challenging 10-frame interval, MBPTrack suffers from compounded errors, leading to severe misalignment. MambaTrack3D demonstrates superior robustness, preserving tracking continuity through sparse yet discriminative temporal fusion.

E. Results on Normal Tracking

Table III compares MambaTrack3D with state-of-the-art (SOTA) trackers on the standard KITTI dataset, where frame-by-frame annotations are available and temporal variation is relatively small. Overall, MambaTrack3D achieves a mean success/precision of 70.0/87.9, which is on par with the

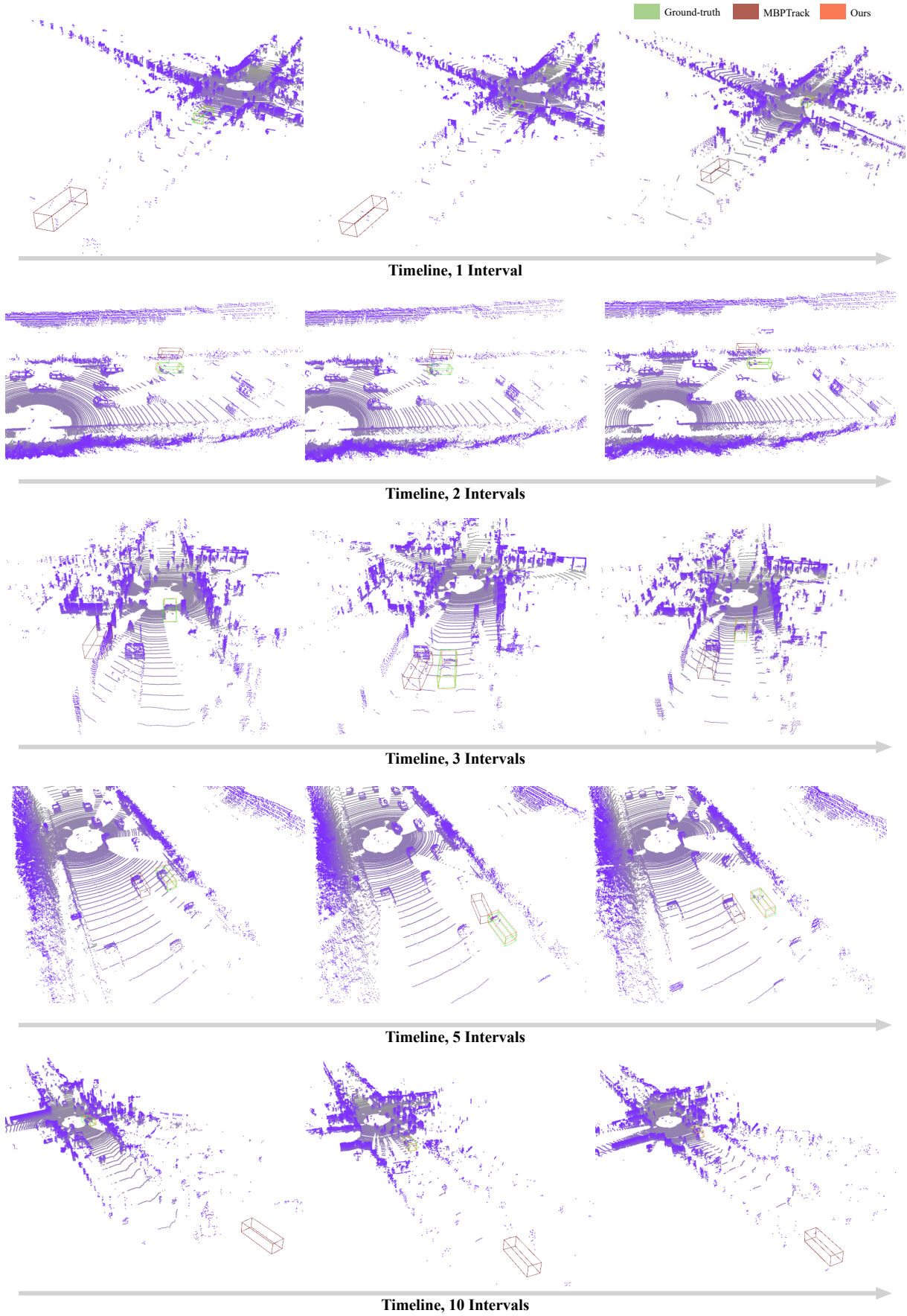


Fig. 5. Visualization of Tracking results on KITTI. We plot five tracklets with different temporal interval, *i.e.*, interval=1, 2, 3, 5, 10. MambaTrack3D is highlighted in orange, and the ground-truth in green. The best view can zoom-in.

TABLE III
COMPARISON OF MAMBATRACK3D WITH THE SOTA METHODS ON EACH CATEGORY OF THE KITTI DATASET.

Methods (Frame Number)	Car (6424)	Pedestrian (6088)	Van (1248)	Cyclist (308)	Mean (14068)
P2B [9]	56.2/72.8	28.7/49.6	40.8/48.4	32.1/44.7	42.4/60.0
MLVSNet [49]	56.0/74.0	34.1/61.1	52.0/61.4	34.3/44.5	45.7/66.7
BAT [25]	60.5/77.7	42.1/70.1	52.4/67.0	33.7/45.4	51.2/72.8
PTT [26]	67.8/81.8	44.9/72.0	43.6/52.5	37.2/47.3	55.1/74.2
V2B [29]	70.5/81.3	48.3/73.5	50.1/58.0	40.8/49.7	58.4/75.2
PTTR [28]	65.2/77.4	50.9/81.6	52.5/61.8	65.1/90.5	57.9/78.1
STNet [10]	72.1/84.0	49.9/77.2	58.0/70.6	73.5/93.7	61.3/80.1
TAT [17]	72.2/83.3	57.4/84.4	58.9/69.2	74.2/93.9	64.7/82.8
M2Track [31]	65.5/80.8	61.5/88.2	53.8/70.7	73.2/93.5	62.9/83.4
CXTrack [16]	69.1/81.6	67.0/91.5	60.0/71.8	74.2/94.3	67.5/85.3
MBPTrack [11]	73.4/84.8	68.6/93.9	61.3/72.7	76.7/94.3	70.3/87.9
MBPTrack* [11]	72.1/83.5	66.6/91.4	57.8/68.5	76.0/94.4	68.5/85.8
HVTrack [21]	68.2/79.2	64.6/90.6	54.8/63.8	72.4/93.7	65.5/83.1
Ours	71.4/84.3	69.4/94.1	64.0/74.8	78.3/95.2	70.0/87.9

*indicates that the results are obtained by re-training this method on our own computer.

strongest normal-scenario tracker MBPTrack (70.3/87.9) and clearly outperforms HVTrack (65.5/83.1). This demonstrates that our method, although designed for high temporal variation (HTV), maintains strong competitiveness in conventional settings. Compared to HVTrack, MambaTrack3D achieves significant improvements across all categories (+3.2/+5.1 for cars, +4.8/+3.5 for pedestrians), proving that the proposed propagation and grouped feature enhancement modules not only benefit HTV scenarios but also strengthen discriminability in stable frame-by-frame tracking.

When compared to conventional trackers, MambaTrack3D is highly competitive with MBPTrack, the current best-performing method, essentially matching its mean performance. Notably, compared to MBPTrack trained on our own devices, our OTTrack slightly surpasses it in mean success/precision rates (68.5/85.8 vs 70.0/87.9). Moreover, against other strong baselines such as CXTrack (67.5/85.3) and M2Track (62.9/83.4), MambaTrack3D shows clear improvements, particularly in the Van and Cyclist categories.

By jointly analyzing Table I and Table III, MambaTrack3D demonstrates dual capability: it excels in high temporal variation scenarios while remaining highly competitive in conventional frame-by-frame tracking. The results validate that our temporal propagation and feature enhancement strategies generalize well, providing robustness across both specialized and normal tracking settings.

F. Ablation Studies

Effect of memory bank size ρ . This paper proposes a point cloud tracking framework based on a state space model, which naturally merges the two-stage process of feature extraction and template embedding into a single-stage historical information propagation. Considering the number of past frames stored may influence the tracking performance, we conduct a

self-comparison experiment on the KITTI dataset to evaluate the effect of the memory bank capacity.

As shown in Table IV, when ρ increases from 1 to 3, both success rate (SR) and precision rate (PR) improve steadily for both car and pedestrian categories. For example, in the pedestrian class, SR/PR rises from 33.7/49.2 at $\rho = 1$ to 39.5/60.1 at $\rho = 3$. These results indicate that incorporating a moderate number of historical frames provides richer temporal cues and enhances discriminability. However, when the memory size is further enlarged ($\rho = 4$ or $\rho = 5$), performance begins to decline. For example, in the car category, the success rate drops from 62.7 at $\rho = 3$ to 59.9 at $\rho = 5$. This degradation suggests that excessive historical information introduces redundancy and noise, which may dilute the relevance of features aligned with the current frame.

TABLE IV
THE SELF-COMPARISON RESULTS ABOUT THE SIZE OF MEMORY BANK.
“SR” AND “PR” DENOTES SUCCESS AND PRECISION METRICS,
RESPECTIVELY.

Memory Bank Size	Car		Pedestrian	
	SR(%)	PR(%)	SR(%)	PR(%)
$\rho = 1$	60.3	70.2	33.7	49.20
$\rho = 2$	61.1	72.1	39.2	58.3
$\rho = 3$	62.7	72.8	39.5	60.1
$\rho = 4$	61.6	71.5	38.6	57.6
$\rho = 5$	59.9	71.1	38.9	57.8

Impact of the number of neighbor point set $\mathcal{N}(q_j)$. For each tracking instance, we maintain a queue-structured memory bank over time. Due to view changes and occlusions, not every historical point is informative. To reduce redundancy, we construct a local neighbor in the same coordinate system via KNN. We investigate how the number of neighbors affects tracking performance. As shown in Figure 6, setting $|\mathcal{N}(q_j)| = 4$ yields the highest success and precision, reaching 62.7/72.8 (Success/Precision). Setting $|\mathcal{N}(q_j)| = 2$ also produces competitive results (61.9/71.3), which demonstrates that even sparse historical support is useful when points are carefully selected. The large $|\mathcal{N}(q_j)|$ expands spatial coverage of historical cues but risks incorporating points affected by pose drift or background contamination. In addition, the narrow range of success (61 ± 1.0) and precision ($\approx 71 \pm 1.0$) across $|\mathcal{N}(q_j)|$ indicates that the pipeline is relatively robust.

Validation of the proposed GFEM. To alleviate redundancy accumulated in the memory bank, we construct local neighborhoods in historical frames and select top-K keypoints. However, since the current frame features are mainly propagated from historical frames, redundant features in the memory bank may lack the discriminability of neighborhood features. To address this issue, we introduce the Grouped Feature Enhancement Module (GFEM), which explicitly separates foreground and background channels to enhance feature representation. Table V reports the validation results of GFEM on the KITTI dataset. Incorporating GFEM consistently improves both success rate (SR) and precision rate (PR) across categories. For Car, SR/PR increases from 60.8/70.4 (w/o GFEM)

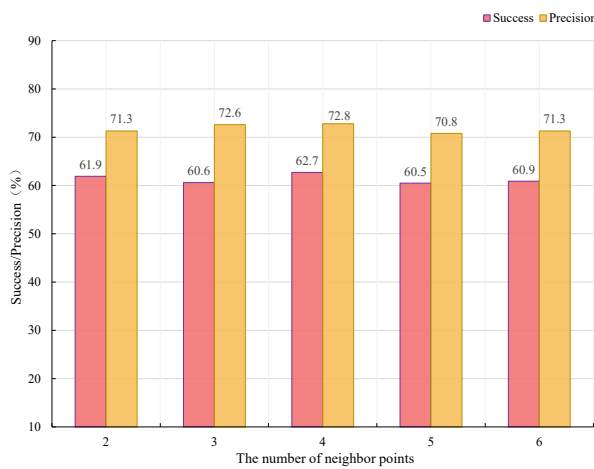


Fig. 6. The impact of the number of neighbors. The results are produced on the car class of KITTI.

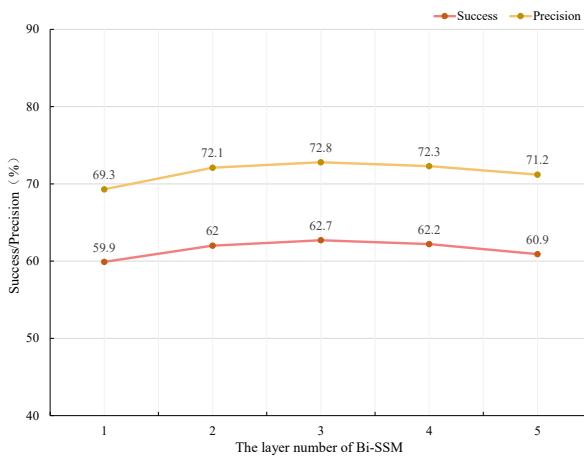


Fig. 7. The self-comparison results of the layer number of Bi-SSM.

to 62.7/72.8 (w/ GFEM). For Pedestrian, the improvement is even more pronounced, rising from 37.0/54.9 to 39.5/60.1.

TABLE V

THE VALIDATION OF THE GROUPED FEATURE ENHANCEMENT MODULE (GFEM). “SR” AND “PR” DENOTES SUCCESS AND PRECISION METRICS, RESPECTIVELY.

Network Architecture	Car		Pedestrian	
	SR(%)	PR(%)	SR(%)	PR(%)
w/ GFEM	62.7	72.8	39.5	60.1
w/o GFEM	60.8	70.4	37.0	54.9

Impact of the layer number of Bi-SSM. We employ a bidirectional state space model (Bi-SSM) to propagate features across frames. To assess architectural depth, we vary the number of Bi-SSM layers from 1 to 5 and report success and precision. As shown in Fig. 7, three Bi-SSM layers provide the best balance between temporal information propagation and robustness. A single layer underfits temporal relations (59.9/69.3), while 2 layers substantially improve both metrics

(62.0/72.1), showing clear gains from modest depth. Increasing to 4 layers maintains precision (72.3) but slightly reduces success (62.2), and 5 layers further degrades both metrics (60.9/71.2). This suggests deeper stacks introduce redundant or misaligned temporal cues that weaken correspondence quality. We adopted $L = 3$ as the default configuration.

TABLE VI

THE SELF-COMPARISON RESULTS OF ONLY USING GEOMETRIC FEATURES AND SEMANTIC MASK FEATURES. “SR” AND “PR” DENOTES SUCCESS AND PRECISION METRICS, RESPECTIVELY.

Geometric Feat.	Mask Feat.	Car		Pedestrian	
		SR(%)	PR(%)	SR(%)	PR(%)
✓		61.9	71.8	37.0	55.2
	✓	52.0	62.1	36.6	56.5
✓	✓	62.7	72.8	39.5	60.1

Effect of geometric and mask semantic information.

In Eq. (6), both geometric features of point clouds and semantic mask features are fused to enhance discriminability. To validate their complementary roles, we conduct an ablation study by training the model with only one type of feature at a time. When geometric and semantic features are integrated, the model achieves the best performance (62.7/72.8 on Car and 39.5/60.1 on Pedestrian). But when solely relying on geometric information, the model achieves 61.9/71.8 (SR/PR) on Car and 37.0/55.2 on Pedestrian. This indicates that geometric cues provide a solid foundation for rigid objects but are less effective for small or deformable targets. With mask features alone, performance drops significantly for Car (52.0/62.1) but remains comparable for Pedestrian (36.6/56.5). This suggests that semantic cues are helpful for distinguishing small targets, especially in cluttered pedestrian scenes, but insufficient to capture precise geometric structures.

V. CONCLUSION

In this work, we presented MambaTrack3D, a LiDAR-based tracking framework tailored for high temporal variation scenarios. By leveraging the state space model Mamba, our inter-frame propagation module achieves linear-time complexity and effectively exploits spatial-temporal relations across historical frames. To further reduce redundancy, we introduced a grouped feature enhancement module, which enhances discriminability by explicitly modeling foreground-background semantics. Comprehensive experiments on KITTI-HTV and nuScenes-HTV benchmarks validate the effectiveness of our approach. MambaTrack3D consistently surpasses the HTV baseline HVTrack under challenging temporal gaps, while maintaining competitive performance in the normal tracking setting. These results highlight its dual capability: excelling at temporal variation and remaining efficient computation.

Future work will explore extending our framework to class-agnostic [35] or class-unified tracking [50], and integrate adaptive memory management strategies, further enhancing robustness in real-world autonomous driving and robotic perception systems.

ACKNOWLEDGMENT

This work is supported in part by the National Natural Science Foundation of China (Grant No. 62301562), and the China Postdoctoral Science Foundation (Grant No. 2023M733756).

REFERENCES

- [1] X. Ma, J. Bai, Z. Su, and Y. Wang, “Pvstrans: Patch-view-shape progressive interaction transformer for 3d shape recognition,” *Information Processing & Management*, vol. 63, no. 1, p. 104279, 2026.
- [2] Q. Zheng, S. Wu, and J. Wei, “Voxt-gnn: A 3d object detection approach from point cloud based on voxel-level transformer and graph neural network,” *Information Processing & Management*, vol. 62, no. 4, p. 104155, 2025.
- [3] A. I. Comport, É. Marchand, and F. Chaumette, “Robust model-based tracking for robot vision,” in *IEEE/RSJ International Conference on Intelligent Robots and Systems (IROS)*, 2004, pp. 692–697.
- [4] E. Machida, M. Cao, T. Murao, and H. Hashimoto, “Human motion tracking of mobile robot with kinect 3d sensor,” in *Proceedings of SICE Annual Conference (SICE)*, 2012, pp. 2207–2211.
- [5] M.-F. Chang, J. Lambert, P. Sangkloy, J. Singh, S. Bak, A. T. Hartnett, D. Wang, P. Carr, S. Lucey, D. Ramanan, and J. Hays, “Argoverse: 3d tracking and forecasting with rich maps,” in *CVPR*, 2019, pp. 8740–8749.
- [6] A. Geiger, P. Lenz, C. Stiller, and R. Urtasun, “Vision meets robotics: The KITTI dataset,” *International Journal of Robotics Research*, vol. 32, no. 11, pp. 1231–1237, 2013.
- [7] T. A. Syed, M. S. Siddiqui, H. B. Abdullah, S. Jan, A. Namoun, A. Alzahrani, A. Nadeem, and A. B. Alkhodre, “In-depth review of augmented reality: Tracking technologies, development tools, ar displays, collaborative ar, and security concerns,” *Sensors*, vol. 23, no. 1, p. 146, 2022.
- [8] H. Caesar, V. Bankiti, A. H. Lang, S. Vora, V. E. Lioing, Q. Xu, A. Krishnan, Y. Pan, G. Baldan, and O. Beijbom, “nuscenes: A multimodal dataset for autonomous driving,” in *CVPR*, 2020, pp. 11 621–11 631.
- [9] H. Qi, C. Feng, Z. Cao, F. Zhao, and Y. Xiao, “P2B: Point-to-box network for 3d object tracking in point clouds,” in *CVPR*, 2020, pp. 6328–6337.
- [10] L. Hui, L. Wang, L. Tang, K. Lan, J. Xie, and J. Yang, “3d siamese transformer network for single object tracking on point clouds,” in *ECCV*, 2022, pp. 293–310.
- [11] T. Xu, Y. Guo, Y. Lai, and S. Zhang, “Mbptrack: Improving 3d point cloud tracking with memory networks and box priors,” in *2023 IEEE/CVF International Conference on Computer Vision (ICCV)*, 2023, pp. 9877–9886.
- [12] K. Yang, J. Yi, K. Lee, and Y. Lee, “Flexpatch: Fast and accurate object detection for on-device high-resolution live video analytics,” in *IEEE INFOCOM 2022 - IEEE Conference on Computer Communications*, 2022, pp. 1898–1907.
- [13] L. Liu, H. Li, and M. Gruteser, “Edge assisted real-time object detection for mobile augmented reality,” in *Proceedings of the 25th Annual International Conference on Mobile Computing and Networking*, 2019.
- [14] K. Apicharttrisorn, X. Ran, J. Chen, S. V. Krishnamurthy, and A. K. Roy-Chowdhury, “Frugal following: power thrifty object detection and tracking for mobile augmented reality,” in *Proceedings of the 17th Conference on Embedded Networked Sensor Systems*, 2019, pp. 96–109.
- [15] S. Giancola, J. Zarzar, and B. Ghanem, “Leveraging shape completion for 3D Siamese tracking,” in *CVPR*, 2019, pp. 1359–1368.
- [16] T.-X. Xu, Y.-C. Guo, Y.-K. Lai, and S.-H. Zhang, “Cxtrack: Improving 3d point cloud tracking with contextual information,” in *Proceedings of the IEEE/CVF Conference on Computer Vision and Pattern Recognition*, 2023, pp. 1084–1093.
- [17] K. Lan, H. Jiang, and J. Xie, “Temporal-aware Siamese tracker: Integrate temporal context for 3D object tracking,” in *Proceedings of the Asian Conference on Computer Vision*, 2022, pp. 399–414.
- [18] J. Ra, M. Wang, J. Mei, S. Liu, Y. Yang, and Y. Liu, “Exploit spatiotemporal contextual information for 3d single object tracking via memory networks,” in *2024 International Conference on 3D Vision (3DV)*, 2024, pp. 842–851.
- [19] Y. Lin, Z. Li, Y. Cui, and Z. Fang, “Seqtrack3d: Exploring sequence information for robust 3d point cloud tracking,” in *2024 IEEE International Conference on Robotics and Automation (ICRA)*, 2024, pp. 6959–6965.
- [20] A. Vaswani, N. Shazeer, N. Parmar, J. Uszkoreit, L. Jones, A. N. Gomez, L. Kaiser, and I. Polosukhin, “Attention is all you need,” in *Proceedings of the 31st International Conference on Neural Information Processing Systems*, 2017, p. 6000–6010.
- [21] Q. Wu, K. Sun, P. An, M. Salzmann, Y. Zhang, and J. Yang, “3d single-object tracking in point clouds with high temporal variation,” in *ECCV*. Springer Nature Switzerland, 2025, pp. 279–296.
- [22] A. Gu and T. Dao, “Mamba: Linear-time sequence modeling with selective state spaces,” *arXiv preprint arXiv:2312.00752*, 2023.
- [23] C. R. Qi, H. Su, K. Mo, and L. J. Guibas, “PointNet: Deep learning on point sets for 3D classification and segmentation,” in *CVPR*, 2017, pp. 77–85.
- [24] C. R. Qi, O. Litany, K. He, and L. J. Guibas, “Deep hough voting for 3D object detection in point clouds,” in *IEEE/CVF International Conference on Computer Vision (ICCV)*, 2019, pp. 9277–9286.
- [25] C. Zheng, X. Yan, J. Gao, W. Zhao, W. Zhang, Z. Li, and S. Cui, “Box-Aware feature enhancement for single object tracking on point clouds,” in *ICCV*, 2021, pp. 13 199–13 208.
- [26] J. Shan, S. Zhou, Y. Cui, and Z. Fang, “Real-time 3d single object tracking with transformer,” *IEEE Transactions on Multimedia*, vol. 25, pp. 2339–2353, 2023.
- [27] M. Park, H. Seong, W. Jang, and E. Kim, “Graph-based point tracker for 3d object tracking in point clouds,” in *AAAI Conference on Artificial Intelligence*, 2022, pp. 2053–2061.
- [28] Z. Luo, C. Zhou, L. Pan, G. Zhang, T. Liu, Y. Luo, H. Zhao, Z. Liu, and S. Lu, “Exploring point-bev fusion for 3d point cloud object tracking with transformer,” *IEEE Transactions on Pattern Analysis and Machine Intelligence*, vol. 46, no. 9, pp. 5921–5935, 2024.
- [29] L. Hui, L. Wang, M. Cheng, J. Xie, and J. Yang, “3d siamese voxel-to-bev tracker for sparse point clouds,” in *Advances in Neural Information Processing Systems (NeurIPS)*, 2021, pp. 28 714–28 727.
- [30] Z. Guo, Y. Mao, W. Zhou, M. Wang, and H. Li, “CMT: Context-matching-guided transformer for 3D tracking in point clouds,” in *European Conference on Computer Vision*. Springer, 2022, pp. 95–111.
- [31] C. Zheng, X. Yan, H. Zhang, B. Wang, S. Cheng, S. Cui, and Z. Li, “An effective motion-centric paradigm for 3d single object tracking in point clouds,” *IEEE Transactions on Pattern Analysis and Machine Intelligence*, vol. 46, no. 1, pp. 43–60, 2024.
- [32] J. Nie, F. Xie, S. Zhou, X. Zhou, D.-K. Chae, and Z. He, “P2p: Part-to-part motion cues guide a strong tracking framework for lidar point clouds,” *International Journal of Computer Vision*, vol. 133, no. 8, p. 5326–5342, 2025. [Online]. Available: <https://doi.org/10.1007/s11263-025-02430-6>
- [33] Y. Xia, Q. Wu, W. Li, A. B. Chan, and U. Stilla, “A lightweight and detector-free 3d single object tracker on point clouds,” *IEEE Transactions on Intelligent Transportation Systems*, vol. 24, no. 5, pp. 5543–5554, 2023.
- [34] Z. Luo, G. Zhang, C. Zhou, Z. Wu, Q. Tao, L. Lu, and S. Lu, “Modeling continuous motion for 3d point cloud object tracking,” in *Proceedings of the AAAI Conference on Artificial Intelligence*, vol. 38, no. 5, 2024, pp. 4026–4034.
- [35] S. Tian, J. Liu, and X. Liu, “Toward class-agnostic tracking using feature decorrelation in point clouds,” *IEEE Transactions on Image Processing*, vol. 33, pp. 682–695, 2024.
- [36] S. Tian, Y. Han, X. Zhao, and X. Liu, “Small object tracking in lidar point clouds: Learning the target-awareness prototype and fine-grained search region,” *Sensors*, vol. 25, no. 12, p. 3633, 2025.
- [37] M. Dreissig, D. Scheuble, F. Piewak, and J. Boedecker, “Survey on lidar perception in adverse weather conditions,” in *2023 IEEE Intelligent Vehicles Symposium (IV)*. IEEE, 2023, pp. 1–8.
- [38] S. Tian, Y. Han, X. Zhao, B. Liu, and X. Liu, “Evaluating the robustness of lidar point cloud tracking against adversarial attack,” *arXiv preprint arXiv:2410.20893*, 2024.
- [39] T. Dao and A. Gu, “Transformers are SSMs: Generalized models and efficient algorithms through structured state space duality,” in *International Conference on Machine Learning (ICML)*, 2024.
- [40] A. Gu, K. Goel, and C. Ré, “Efficiently modeling long sequences with structured state spaces,” in *The International Conference on Learning Representations (ICLR)*, 2022.
- [41] A. Hatamizadeh and J. Kautz, “Mambavision: A hybrid mamba-transformer vision backbone,” in *Proceedings of the IEEE/CVF Conference on Computer Vision and Pattern Recognition (CVPR)*, June 2025, pp. 25 261–25 270.
- [42] W. Yu and X. Wang, “Mambaout: Do we really need mamba for vision?” in *Proceedings of the IEEE/CVF Conference on Computer Vision and Pattern Recognition (CVPR)*, 2025, pp. 4484–4496.

- [43] D. Liang, X. Zhou, W. Xu, X. Zhu, Z. Zou, X. Ye, X. Tan, and X. Bai, “Pointmamba: A simple state space model for point cloud analysis,” in *Advances in Neural Information Processing Systems*, vol. 37. Curran Associates, Inc., 2024, pp. 32 653–32 677.
- [44] X. Jin, H. Su, K. Liu, C. Ma, W. Wu, F. Hui, and J. Yan, “Unimamba: Unified spatial-channel representation learning with group-efficient mamba for lidar-based 3d object detection,” in *Proceedings of the Computer Vision and Pattern Recognition Conference (CVPR)*, 2025, pp. 1407–1417.
- [45] T. Zhang, H. Yuan, L. Qi, J. Zhang, Q. Zhou, S. Ji, S. Yan, and X. Li, “Point cloud mamba: Point cloud learning via state space model,” in *Proceedings of the AAAI Conference on Artificial Intelligence*, vol. 39, no. 10, Apr. 2025, pp. 10 121–10 130.
- [46] X. Han, Y. Tang, Z. Wang, and X. Li, “Mamba3d: Enhancing local features for 3d point cloud analysis via state space model,” in *Proceedings of the 32nd ACM International Conference on Multimedia*, 2024, pp. 4995–5004.
- [47] M. Kristan, J. Matas, A. Leonardis, T. Vojíř, R. Pflugfelder, G. Fernandez, G. Nebehay, F. Porikli, and L. Čehovin, “A novel performance evaluation methodology for single-target trackers,” *IEEE transactions on pattern analysis and machine intelligence*, vol. 38, no. 11, pp. 2137–2155, 2016.
- [48] J. Liu, Y. Wu, M. Gong, Q. Miao, W. Ma, C. Xu, and C. Qin, “M3sot: Multi-frame, multi-field, multi-space 3d single object tracking,” in *Proceedings of the AAAI Conference on Artificial Intelligence*, vol. 38, no. 4, 2024, pp. 3630–3638.
- [49] Z. Wang, Q. Xie, Y.-K. Lai, J. Wu, K. Long, and J. Wang, “MLVSNet: Multi-level voting siamese network for 3D visual tracking,” in *Proceedings of the IEEE/CVF International Conference on Computer Vision*, 2021, pp. 3101–3110.
- [50] M. Wang, H. Wang, Y. Li, X. Kong, J. Du, G. Shen, and F. Xia, “Trackany3d: Transferring pretrained 3d models for category-unified 3d point cloud tracking,” in *Proceedings of the IEEE International Conference on Computer Vision (ICCV)*, 2025.